# Crystallinity and Cross-Linking in Porous Polymers Synthesized from Long Side Chain Monomers through Emulsion Templating

# Shulamit Livshin and Michael S. Silverstein\*

Department of Materials Engineering, Technion—Israel Institute of Technology, Haifa 32000, Israel Received January 27, 2008; Revised Manuscript Received March 13, 2008

ABSTRACT: A polyHIPE is a cross-linked, porous polymer synthesized through polymerization in the external phase of a high internal phase emulsion (HIPE). Crystalline polyHIPE polymers were synthesized through copolymerization of stearyl acrylate and divinylbenzene (DVB). Polymerizations initiated at the water/organic interface were compared to equivalent bulk polymers, to equivalent polymerizations initiated in the organic phase, and to model copolymers containing an equivalent non-cross-linking comonomer (styrene). The higher of the two main melting endotherms was related to a more ordered crystalline structure formed by stearyl acrylate-rich molecular segments that are preferentially synthesized by initiation at the interface. Cross-linking restricts molecular mobility, tying the polymer backbones together and reducing the peak temperatures and crystallinities. The decrease in modulus with increasing DVB content for the more crystalline polyHIPE reflects the dominant effect of crystallinity. The increase in modulus with increasing DVB content for the less crystalline polyHIPE reflects the dominant effects of cross-linking and polymer backbone stiffness.

#### Introduction

A high internal phase emulsion (HIPE) has been defined as an emulsion in which the internal phase occupies more than 74% of the volume. A polyHIPE is a highly cross-linked, porous polymer that results from polymerizing monomers and crosslinking comonomers in the external phase of a HIPE. 1-5 Significant amounts of a cross-linking comonomer are used to prevent polyHIPE collapse during polymerization and drying. A variety of polyHIPE and polyHIPE-based materials have been synthesized including copolymers, <sup>1-8</sup> interpenetrating polymer networks (IPN), <sup>9</sup> hydrogels, <sup>10–12</sup> biocompatible polymers, <sup>13–19</sup> organic—inorganic hybrids, <sup>20,21</sup> and composites. <sup>22–28</sup> Porous materials have numerous applications in such areas as catalysis, chromatography, and separation, where control over pore structure and pore size strongly influences the efficiency of the material.<sup>29</sup> PolyHIPE, with their high porosities, high degrees of interconnectivity, and unique micrometer- to nanometer-scale open-pore structures, have been investigated for such applications.

PolyHIPE are usually synthesized from monomers which yield amorphous homopolymers. Even monomers which could yield crystalline homopolymers are not likely to crystallize in polyHIPE, owing to the significant amounts of cross-linking comonomer. The cross-linking comonomer disrupts the structural regularity of the polymer backbone, restricts polymer mobility, and limits the ability of the backbone to organize into an ordered, crystalline structure.

Previous research has shown that it is possible to synthesize crystallizable polyHIPE through the polymerization of monomers with crystallizable side chains. The side chains are flexible enough to crystallize in regions far from the polymer backbone. The side chain monomers investigated were either acrylates or methacrylates. The n-alkyl side chains investigated were either  $C_{12}$  or  $C_{18}$ . The densities (around 0.11 g/cm<sup>3</sup>) and the porous structures of these porous polymers were typical of polyHIPE. All the polyHIPE synthesized using side chain monomers exhibited melting peaks. The melting peak temperatures ( $T_{\rm m}$ ) and the crystallinities ( $X_{\rm c}$ ) were higher for the acrylates than for the methacrylates, reflecting the higher

molecular mobilities of the acrylate backbones that promoted the formation of a more ordered crystalline structure.  $T_{\rm m}$  and  $X_{\rm c}$  were higher for the  $C_{18}$  side chains than for the  $C_{12}$  side chains, reflecting the ability of the longer side chains to organize into a more ordered crystalline structure. The only polyHIPE to exhibit a significant crystallinity above room temperature was based on an acrylate with a  $C_{18}$  side chain. This higher temperature crystalline phase had a Bragg d-spacing of 4.20 Å, typical of paraffin-like hexagonal lattices.<sup>31</sup>

Copolymerization with a non-cross-linking comonomer can disrupt side chain organization and impede crystallization.  $^{34-37}$  As a result, the  $T_{\rm m}$  and  $X_{\rm c}$  of the side chain crystalline structures formed in copolymers are lower than those of the crystalline structures formed in homopolymer. Copolymerization with a cross-linking comonomer is expected to cause a greater disruption in side chain organization, impeding crystallization even further and yielding more significant reductions in  $T_{\rm m}$  and  $X_{\rm c}$ .

This research describes the effects of cross-linking on the side chain crystallinity of polyHIPE. The influences of the comonomer content and of the locus of initiation on the polyHIPE molecular structure, porous morphology, and properties were investigated. In addition, the synthesis within HIPE of model non-cross-linked copolymers based on an equivalent non-cross-linking comonomer is described. The relationships between the synthesis parameters and the crystallinities are described and discussed.

## **Experimental Section**

Materials. The monomers with C<sub>18</sub> side chains were stearyl acrylate (A18, with a melting point of 34 °C, Sigma-Aldrich) and stearyl methacrylate (M18, with a melting point of 19 °C, Sigma-Aldrich). The cross-linking comonomer was divinylbenzene containing 40% ethylstyrene (DVB, Riedel-Haen). The non-cross-linking comonomer was styrene (S, Fluka Chemie). The inhibitors in S and DVB were removed through extraction with 1.25 M sodium hydroxide (NaOH, Sigma-Aldrich). A18 and M18 were used as received. For polyHIPE synthesis, the organic-soluble emulsifier was sorbitan monooleate (SMO, Span 80, Fluka Chemie), the water-soluble initiator was potassium persulfate (KPS, Riedel-Haen), and the stabilizer was potassium sulfate (K<sub>2</sub>SO<sub>4</sub>, Frutarom, Israel). The organic-soluble initiator used for bulk polymerization (as well as for some exceptional HIPE syntheses) was benzoyl peroxide (BPO, Fluka Chemie). The solvents used were toluene

<sup>\*</sup> To whom correspondence should be addressed: e-mail michaels@tx.technion.ac.il, Tel 972-4-829-4582, Fax 972-4-829-5677.

Table 1. HIPE Compositions and PolyHIPE Properties

polyHIPE	monomer	comonomer	initiator	comonomer, mol %	ρ, g/cm <sup>3</sup>	A, m²/g
A18-X0	A18		KPS	0		
A18-X0-O	A18		BPO	0		
A18-D12	A18	DVB	KPS	12	0.16	0.2
A18-D22	A18	DVB	KPS	22	0.11	2.1
A18-D38	A18	DVB	KPS	38	0.11	1.4
A18-D38-P	A18	DVB	BPO + KPS	38	0.11	
A18-D38-O	A18	DVB	BPO	38	0.14	3.0
A18-D50	A18	DVB	KPS	50	0.11	4.5
A18-D62	A18	DVB	KPS	62	0.10	2.7
A18-S38	A18	S	KPS	38		
A18-S38-O	A18	S	BPO	38		
M18-D22	M18	DVB	KPS	22	0.12	
M18-D39	M18	DVB	KPS	39	0.11	4.0

Table 2. Typical Recipes for A18-D38-Based PolyHIPE

	component	amount, wt %				
phase		A18-D38	A18-D38-P	A18-D38-O	A18-D38-B	
organic	A18	7.79	7.77	7.79	78.43	
	DVB	1.95	1.94	1.95	19.61	
	SMO	1.95	1.94	1.95		
	BPO	0.00	0.19	0.19	1.96	
	total	11.68	11.86	11.88	100.00	
aqueous	water	87.63	87.46	87.63		
•	KPS	0.19	0.19	0.00		
	$K_2SO_4$	0.49	0.49	0.49		
	total	88.32	88.14	88.12		

(Frutarom, Israel), methanol (Frutarom, Israel), deuterated chloroform (CDCl<sub>3</sub>, Aldrich), and tetrahydrofuran (THF, HPLC grade, Labscan).

Standard PolyHIPE Synthesis. In the standard polyHIPE synthesis, the initiator was KPS and initiation took place at the organic-water interface. The standard polyHIPE in Table 1 are labeled either A18-Dx or M18-Dx, where A18 and M18 are the side chain monomers, D indicates DVB, and x indicates the molar percentage of DVB from the total monomer content. A typical recipe used for standard polyHIPE synthesis (A18-D38) is listed in Table 2.

The organic phase (monomers and emulsifier) and the aqueous phase (water, KPS, and stabilizer) were each mixed separately. A18 was heated to 40 °C both for mixing and for HIPE formation. HIPE were formed by adding the aqueous phase (about 90% of the total volume) dropwise to the organic phase (about 10% of the total volume) with constant stirring. The resulting HIPE were covered with a plastic film, and polymerization took place in a circulating air oven at 65 °C for 18 h. The water was removed from the polyHIPE by drying at room temperature in a vacuum oven until a constant weight was reached (about 3 days). The emulsifier, initiator, and stabilizer were removed by Soxhlet extraction, first in deionized water for 24 h and then in methanol for 24 h. The polyHIPE was then dried in a vacuum oven at room temperature for 24 h. The resulting polyHIPE were all white, porous monoliths. The yield is the polymer (following Soxhlet extraction and drying) to monomer feed mass ratio.

Prepolymerization, Organic Phase Initiation, and Non-Cross-Linked Polymers. In prepolymerized polyHIPE, A18 (with no DVB) underwent partial polymerization before the HIPE was formed. A18 containing 2 wt % BPO was placed in a circulating air oven at 65 °C for 30 min. Prepolymerization of monomer mixtures that included DVB were not used since prepolymerization could lead to gelation and prevent the formation of a HIPE. Following prepolymerization, the remaining components were added to the organic phase. The aqueous phase containing KPS was then added dropwise, and the synthesis proceeded as described above for the standard polyHIPE synthesis. The labels for the prepolymerized polyHIPE bear the suffix "P". A typical recipe (A18-D38-P) is listed in Table 2.

The locus of initiation was changed from the organic-water interface to within the organic phase by replacing the KPS in the aqueous phase with BPO in the organic phase. Except for this change in the recipe, the synthesis proceeded as described above for the standard polyHIPE synthesis. The labels for the organic phase initiated polyHIPE bear the suffix "O". A typical recipe (A18-D38-O) is listed in Table 2. The prepolymerized and organic phase initiated polyHIPE were all white, porous monoliths.

Polymers that were not cross-linked were also synthesized within HIPE. Both the standard polyHIPE synthesis procedure and the organic phase initiated synthesis procedure were used to synthesize these non-cross-linked polymers. A18 homopolymers (A18-X0 and A18-X0-O) were synthesized within HIPE that contained A18 but did not contain comonomers. Model non-cross-linked copolymers were synthesized within HIPE that contained both A18 and styrene. Styrene was used as a non-cross-linking equivalent of DVB. The copolymers with styrene are labeled A18-Sx, where S is styrene and x is the molar percentage of styrene from the total monomer content. The non-cross-linked polymers disintegrated into a powder upon drying. The powders were dissolved in toluene, precipitated in methanol, and dried in a vacuum oven at room temperature for 24 h.

Bulk Synthesis. The polyHIPE were compared with polymers of the same comonomer compositions synthesized through bulk polymerization. The BPO content was 2 wt % of the monomer content. The comonomers were heated to 40 °C in order to melt the A18 and enhance miscibility. Polymerization took place in a circulating air oven at 65 °C for 18 h. The polymers were dissolved in toluene, precipitated in methanol, and dried in a vacuum oven for 24 h. The labels for the bulk polymerized polymers bear the suffix "B". A typical recipe used for bulk polymerization (A18-D38-B) is listed in Table 2.

**Characterization.** The polyHIPE densities,  $\rho$ , were determined by gravimetric analysis. The specific surface areas, A, were determined by the single-point BET (Brunauer, Emmett, Teller) method with nitrogen adsorption-desorption at 77 K (Flowsorb II, Micromeritics). The porous structures of cryogenic facture surfaces were investigated using high-resolution scanning electron microscopy (HRSEM, Zeiss LEO 982). The samples, viewed using an accelerating voltage of 4 kV, were not coated. The ranges of void and hole diameters were determined by analyzing the SEM images and using a statistical correction to account for the arbitrary, nonequatorial, location of the section.<sup>38</sup> The crystalline structure was investigated using X-ray diffraction (XRD, Philips PW 1840 X-ray) with a Ni-filtered Cu Ka X-ray beam excited at 40 kV and

The thermal properties ( $T_{\rm m}$  and the heat of the melting endotherm,  $\Delta H$ ) were investigated using differential scanning calorimetry (DSC) Mettler DSC-821 calorimeter). The samples were heated from -120to 120 °C at a rate of 10 °C/min in nitrogen.  $\Delta H$  was normalized by the side chain monomer content and by the side chain monomer molecular weight to yield the heat per mole side chain monomer,  $\Delta H_{\rm SC}$ .  $X_{\rm c}$  was calculated by dividing  $\Delta H_{\rm SC}$  by the number of carbon atoms in the *n*-alkyl side chain and by the heat of fusion of the individual methylene groups, 3.08 kJ/mol for hexagonal packing.33,39,40 Compressive stress-strain measurements were performed at room temperature on  $0.5 \times 0.5 \times 0.5$  cm<sup>3</sup> cubes (DMTA, Rheometrics MKIII) until equipment-related force or displacement limitations were reached. The static compressive moduli, E, were determined from the initial slopes of the compressive stress-strain curves.

The molecular structures of the non-cross-linked polymers were investigated using <sup>1</sup>H nuclear magnetic resonance (NMR, Bruker Avance 500) with CDCl<sub>3</sub> as the solvent. The molecular weights  $(M_n)$  and polydispersity indices (PDI) of the non-cross-linked polymers were determined by gel permeation chromatography (GPC) with THF as the solvent (Waters GPC Breeze). The GPC device is equipped with four columns: three Styragel HR columns (Waters) and one guard column. A refractive index detector is used for molecular weight determination. Seven narrow polystyrene standards with molecular weights in the range of 18 700–890 000 were used for the calibration of the GPC device (Aldrich). The calibration curve was linear in the molecular weight range.

#### **Results and Discussion**

**Porous Structure.** The polymerization yields were all above 90%. The densities of the polyHIPE are presented in Table 1. Most of the polyHIPE have densities of around 0.11 g/cm<sup>3</sup>, as expected from the volume fraction of monomers in the HIPE. The specific surface areas were between 1 and 5 m<sup>2</sup>/g for most of the polyHIPE (Table 1).

The polyHIPE with the lowest DVB content (A18-D12) had a relatively high density, 0.16 g/cm<sup>3</sup>, and a relatively low surface area, 0.2 m<sup>2</sup>/g (Table 1). Previous experience with other acrylates has shown that polyHIPE with low DVB contents tend to collapse during drying. DVB contents of 20 mol % or more are usually needed to prevent this collapse. The DVB both crosslinks the polymer and adds stiff units along the polymer backbone. These changes to the molecular structure enhance the resistance to the capillary forces generated during drying and prevents collapse. A18-D12, which contained only 12 mol % DVB, did not collapse during drying. It did, however, undergo a partial collapse at the higher temperatures used during Soxhlet extraction. This partial collapse produces the relatively high density and the relatively low surface area. The side chain crystallinity in A18-D12 can enhance its resistance to collapse during drying at room temperature. However, at temperatures beyond the  $T_{\rm m}$ , at the Soxhlet extraction temperature, there was no crystalline phase that could enhance the resistance to collapse.

SEM micrographs of representative polyHIPE from the A18-Dx series are presented in Figure 1. A18-D12 (Figure 1a) exhibits a distorted porous structure that reflects its partial collapse on Soxhlet extraction. The porous structures of the polyHIPE with DVB contents from 22 mol % (Figure 1b) to 62 mol % (Figure 1c) are quite similar. The porous structures of these polyHIPE are relatively unaffected by the DVB content. The void diameters range between 5 and 45  $\mu$ m, and the diameters of the holes in the wall range between 0.2 and 5  $\mu$ m.

Crystallinity and Cross-Linking. The DSC thermograms from the A18-Dx series of polyHIPE are seen in Figure 2. The bulk polymers exhibit similar thermograms (not shown). A18-X0-B, the bulk homopolymer, exhibits a melting endotherm with a peak at 58 °C (not shown). All the polyHIPE exhibit at least one main melting endotherm. Some of the polyHIPE exhibit two main melting endotherms. The endotherms whose peaks range between 36 and 46 °C are termed  $T_{\rm m2}$  endotherms. The relative sizes of the  $T_{\rm m2}$  endotherms decrease with increasing DVB content. The endotherms whose peaks range between 7 and 20 °C are termed  $T_{\rm m1}$  endotherms. The relative sizes of the  $T_{\rm m1}$  endotherms increase with increasing DVB content. Most of the A18-Dx polyHIPE also exhibit a very small endotherm,  $T_{\rm m3}$ , at around 60 °C. This endotherm seems to indicate the existence of a small amount of crystallites that are similar to those in the bulk homopolymer.

The variation of the melting peak temperatures with the DVB content is seen in Figure 3, both for the polyHIPE and for the bulk polymers. A18-X0, A18 homopolymerized within a HIPE, exhibits a melting peak at 53 °C, somewhat lower than the 58 °C of the bulk homopolymer. The melting peak temperatures all decrease with increasing DVB content, both for the polyHIPE and for the bulk polymers.  $T_{\rm ml}$  and  $T_{\rm m2}$  decrease somewhat more rapidly for the bulk polymers than for the polyHIPE.

A18-D12 and A18-D12-B do not exhibit a  $T_{\rm m1}$  endotherm. A  $T_{\rm m1}$  endotherm is discernible for DVB contents of 22% and over. There is a significant  $T_{\rm m2}$  endotherm for up to 38% DVB in the polyHIPE, but only for up to 22% DVB in the bulk polymers. The presence of two main endotherms reflects a compositional distribution in the polymer.

While A18 is highly hydrophobic, it does exhibit surface activity and has been used as a cosurfactant in miniemulsions. 41,42 A18 forms stable monolayer films on water with the

ester groups oriented normal to the surface and with close packing of the long n-alkyl side chains. Al8 homopolymers form similar, oriented, monolayer films on water. Al8 This surface activity can yield an Al8-rich environment at the water—organic interface, yielding Al8-rich molecular segments when polymerization is initiated at that interface. The Al8-rich molecular segments would be relatively mobile and could crystallize into a more ordered structure with a higher peak temperature. Molecular segments that are not Al8-rich have a more limited mobility and would crystallize into a less ordered structure with a lower peak temperature. The existence of a significant  $T_{\rm m2}$  endotherm for Al8-D38, but not for Al8-D38-B, indicates that more Al8-rich molecular segments are synthesized in Al8-D38, and these molecular segments can form a more ordered crystalline structure.

The heats of the individual endotherms were determined using curve fitting. The side chain crystallinity based on the  $T_{\rm m2}$  endotherm is termed  $X_{\rm c2}$ , and the side chain crystallinity based on the  $T_{\rm m1}$  endotherm is termed  $X_{\rm c1}$ . The variation of  $X_{\rm c2}$  and  $X_{\rm c1}$  with the DVB content is seen in Figure 4.  $X_{\rm c2}$  decreases with increasing DVB content in a linear fashion.  $X_{\rm c1}$  reaches a plateau of around 22% for DVB contents of 38 mol % and over. The dependence of the total crystallinity,  $X_{\rm cT}$  (the sum of  $X_{\rm c2}$  and  $X_{\rm c1}$ ), on the DVB content can be seen in Figure 5.  $X_{\rm cT}$  in the bulk polymers decreases with increasing DVB content in a linear fashion.  $X_{\rm cT}$  decreases somewhat more rapidly in the bulk polymers than in the polyHIPE. The presence of a  $T_{\rm m2}$  endotherm for A18-D38 but not for A18-D38-B yields a significantly higher  $X_{\rm cT}$  for A18-D38.

At high DVB contents it becomes more likely that not all the DVB serves as a cross-linker, since not all of the double bonds can react. However, the effects of DVB on the peak temperatures and on the crystallinity originate both in the formation of cross-links and in the disruption of the molecular order that allows the side chains to crystallize. For this reason both the peak temperatures and the crystallinities continue to decrease with increasing DVB content.

**Crystalline Structure.** X-ray scattering from the A18-Dx series of polyHIPE is presented in Figure 6. A18-X0 exhibits a crystalline peak at 21.0°, which corresponds to a Bragg d-spacing of 4.20 Å. This Bragg d-spacing is typical of the paraffin-like hexagonal lattices formed by the packing of n-alkyl chains. A18-D50 exhibits an amorphous peak with a maximum at around 18.5° that corresponds to a distance of 4.65 Å, the average distance between disordered (amorphous) n-alkyl chains. The amorphous peak contains a shoulder at around 21° that corresponds to the crystalline peak. The relative area of the crystalline peak decreases, and the relative area of the amorphous peak increases, with increasing DVB content. These changes are consistent with the decrease in  $X_{c2}$ , the more ordered crystalline structure with a peak temperature above room temperature, as described above.

Mechanical Properties. Representative compressive stress—strain curves for the A18-Dx polyHIPE are presented in Figure 7 (A18-D12, A18-D38, and A18-D62). The stress—strain curves for all the polyHIPE except A18-D12 exhibit a linear elastic region at low strains, a stress plateau region, and a densification region with a rapid increase in stress. A18-D12, which underwent partial collapse during extraction, does not exhibit a stress plateau region but, rather, a linear elastic region followed immediately by densification. The variation of the A18-Dx moduli with DVB content is seen in Figure 8.

The relative modulus of a foam (the modulus of the foam divided by the modulus of the wall material) is related to the square of the relative density of the foam (the density of the foam divided by the density of the wall material). 46 A18-D12 has a higher density, crystallinity, and modulus than the other

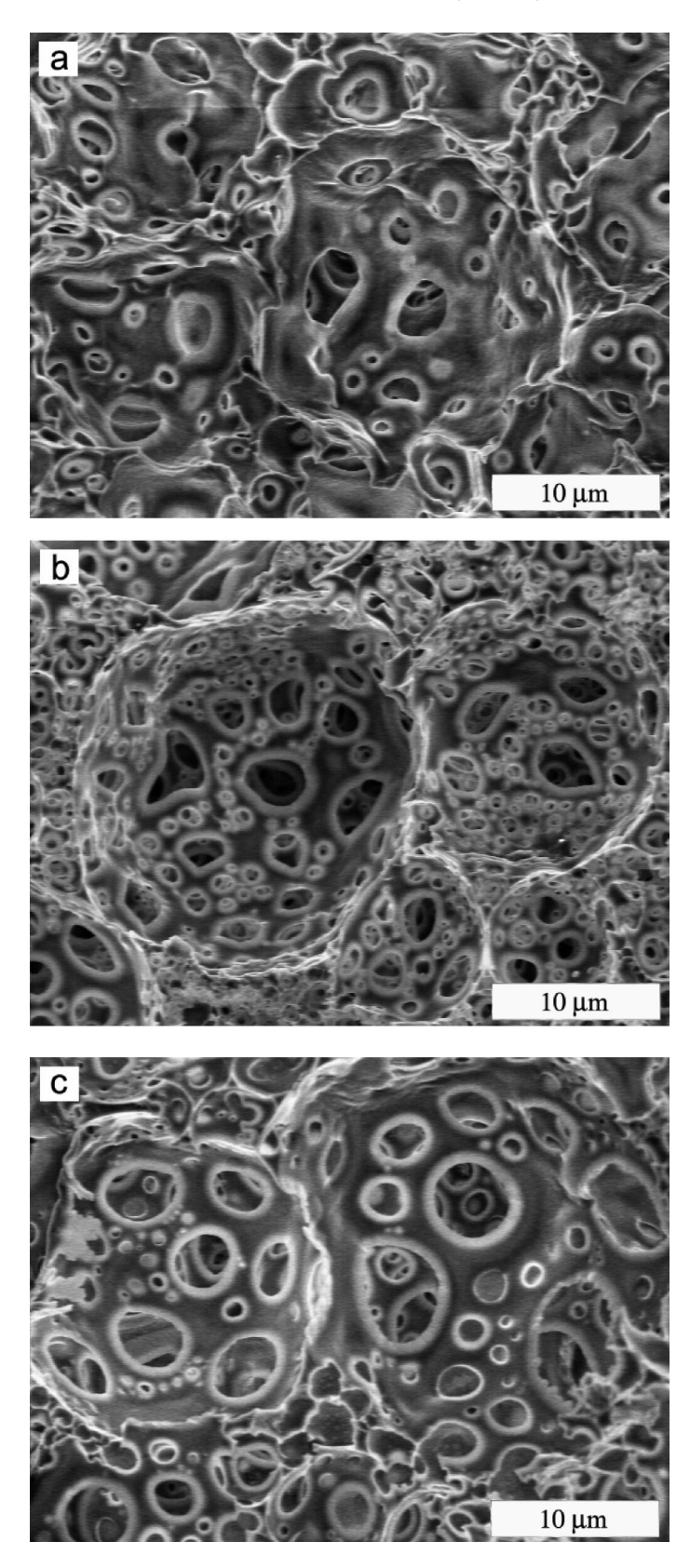


Figure 1. SEM micrographs of polyHIPE fracture surfaces: (a) A18-D12, (b) A18-D22, and (c) A18-D62.

polyHIPE. However, since A18-D12 is significantly more dense than the other polyHIPE, its modulus cannot be compared directly to the moduli of the other polyHIPE. The moduli of polyHIPE with 22 mol % DVB and over, which have similar densities, can be compared directly.

Increasing the DVB content has three interdependent effects. First, the polymer backbone stiffness increases on the incorporation of a relatively stiff comonomer. The increase in backbone stiffness should yield an increase in modulus. Second, the degree of cross-linking increases and should also yield an increase in modulus. Third, the crystallinity decreases which, in contrast, should yield a decrease in modulus. The modulus decreases as the DVB content increases from 22 to 38 mol %. This reduction in modulus indicates that it is the significant decrease in

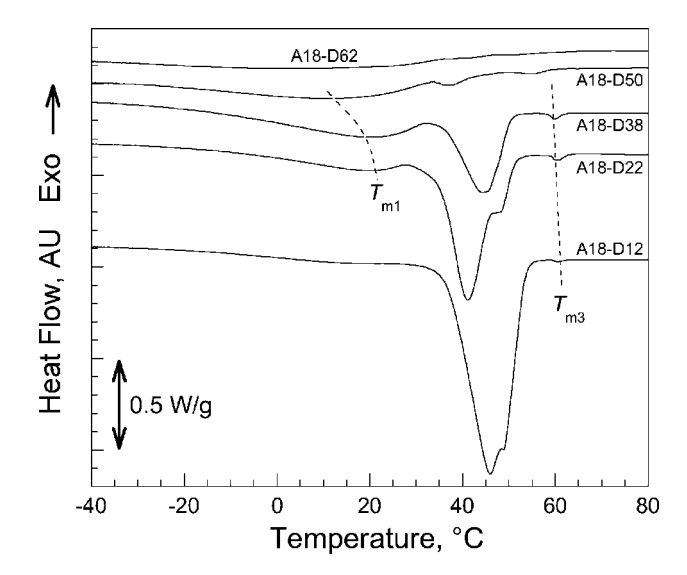
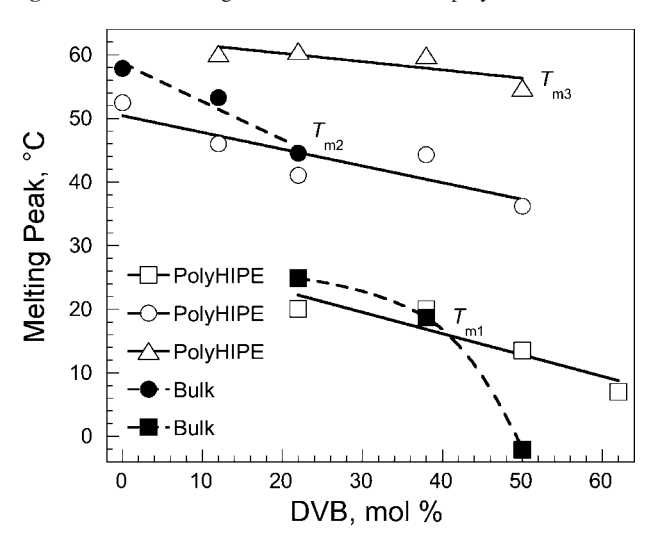
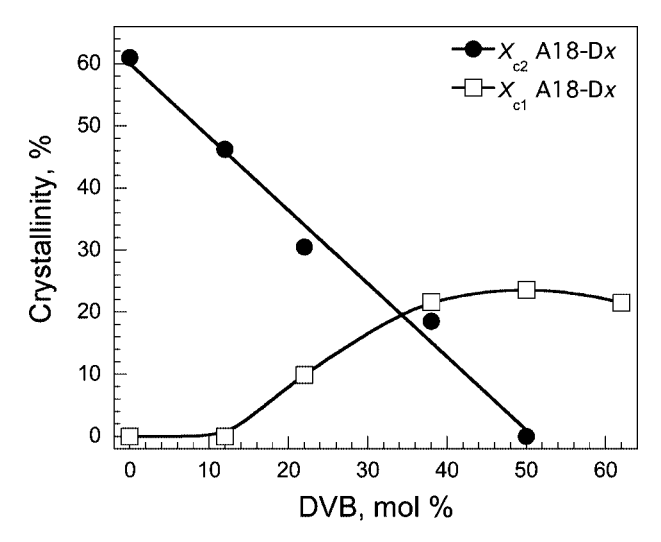


Figure 2. DSC thermograms from the A18-Dx polyHIPE.



**Figure 3.** Variation of the melting peak temperatures with the DVB content for the A18-Dx polyHIPE and for the A18-Dx-B polymers.



**Figure 4.** Variation of  $X_{c1}$  and  $X_{c2}$  with the DVB content for the A18-Dx polyHIPE.

crystallinity that dominates the effects associated with increasing the DVB content for the more crystalline polyHIPE. A18-D38 has a relatively low room temperature crystallinity and an increase in the DVB content yields an increase in modulus. At

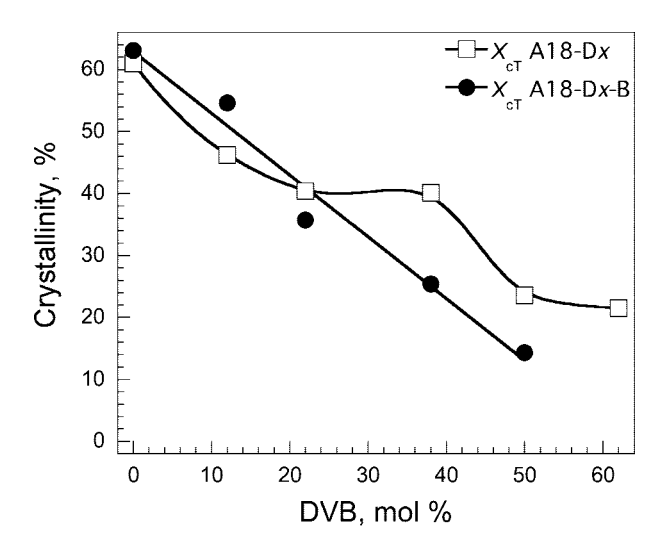


**Figure 5.** Variation of the total crystallinity with the DVB content for the A18-D*x* polyHIPE and for the A18-D*x*-B polymers.

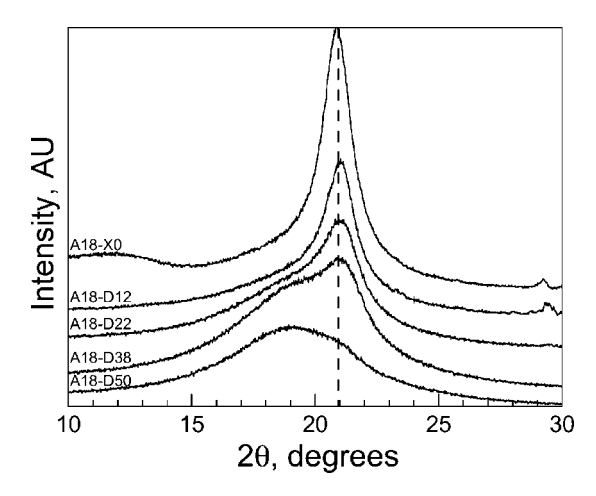


**Figure 6.** X-ray scattering from the A18-Dx polyHIPE.

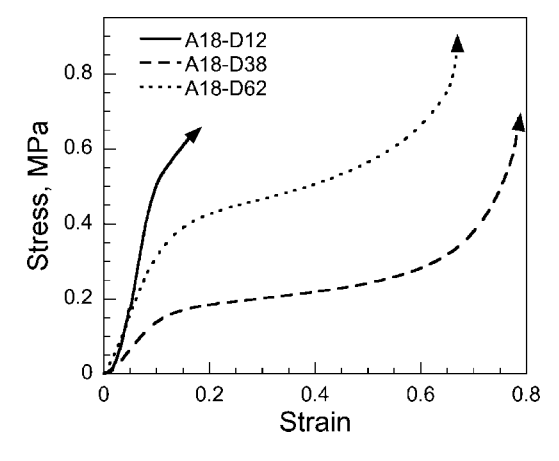


**Figure 7.** Representative compressive stress—strain curves from the A18-Dx polyHIPE.

high DVB contents it becomes more likely that not all the DVB serves as a cross-linker, since not all of the double bonds can react. However, the effects of DVB on the modulus originate both in the formation of cross-links and in the stiffening of the polymer backbone. Therefore, the modulus of the less crystalline polyHIPE at high DVB contents increases with increasing DVB content.

All the M18-Dx polyHIPE are amorphous at room temperature. The stress—strain curves of M18-D22 and M18-D38 are

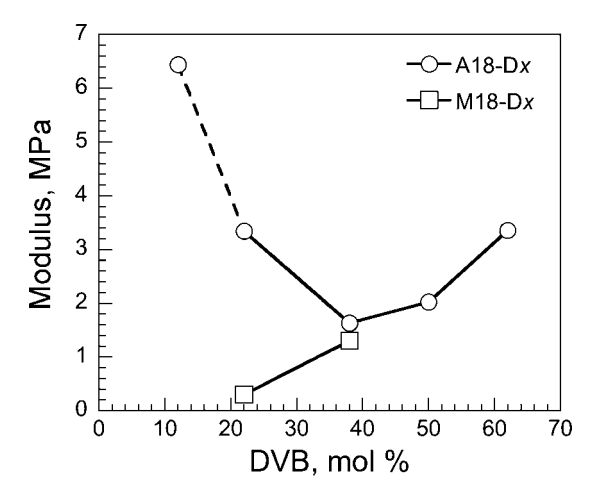
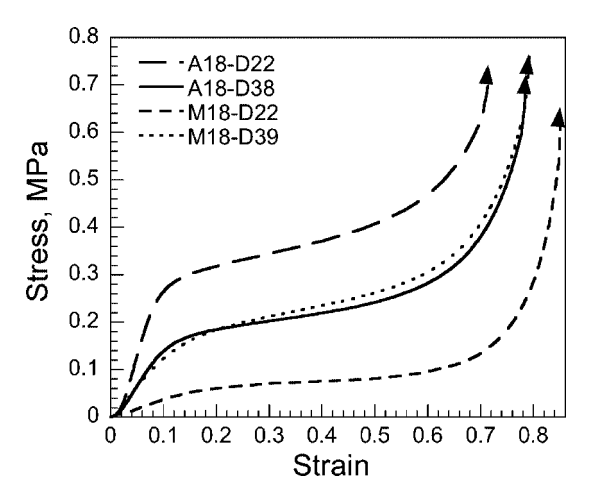


Figure 8. Variation of the modulus with the DVB content for the A18-Dx and M18-Dx polyHIPE.



**Figure 9.** Compressive stress—strain curves for the A18-D22, A18-D38, M18-D22, and M18-D38 polyHIPE.

presented in Figure 9, and the moduli are presented in Figure 8 (the curves for A18-D22 and A18-D38 are also included in Figure 9). The increase in modulus with increasing DVB content for the M18-based polyHIPE reflects the increase in backbone stiffness and the increase in cross-linking. This same increase in DVB content yields the reduction in modulus described above for the more crystalline A18-based polyHIPE.

## Prepolymerized and Organic Phase Initiated PolyHIPE.

The porous morphology of the prepolymerized polyHIPE was quite similar to those of the standard polyHIPE. The polyHIPE synthesized using organic phase initiation exhibited somewhat larger holes and a somewhat higher density of holes than those in the standard polyHIPE. The DSC thermograms of A18-D38-P and A18-D38-O are quite different from that of A18-D38 (Figure 10). The DSC thermograms for A18-D38-P and A18-D38-O are, instead, more similar to that of A18-D38-B (Figure 10). The peak temperatures of the endotherms from these different polyHIPE are compared in Figure 11. The total crystallinities of these different polyHIPE are compared in Figure 12.

Interface initiated A18-D38 exhibits a main melting endotherm at 44 °C and a small additional endotherm at 20 °C (Figure 11). Bulk polymerized (organic phase initiated) A18-D38-B exhibits one melting endotherm, 19 °C, as does the organic phase initiated A18-D38-O polyHIPE, 22 °C (Figure 11). The differences in peak temperature between the two organic phase initiated polymerizations and the  $T_{\rm m1}$  endotherm from initiation at the interface are relatively insignificant. The

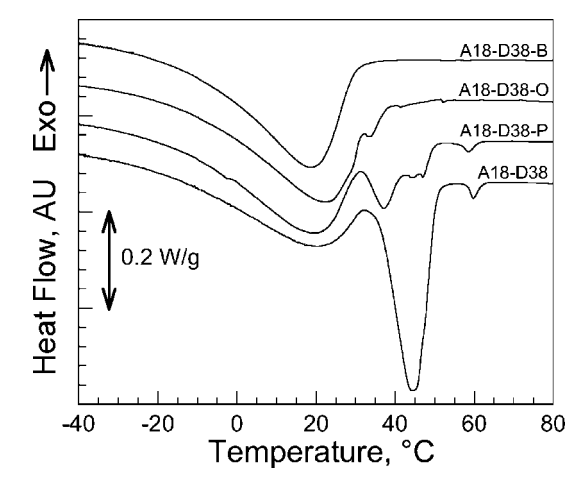


Figure 10. DSC thermograms for various A18-D38-based polymers (bulk polymer as well as standard, prepolymerized, and organic phase initiated polyHIPE).

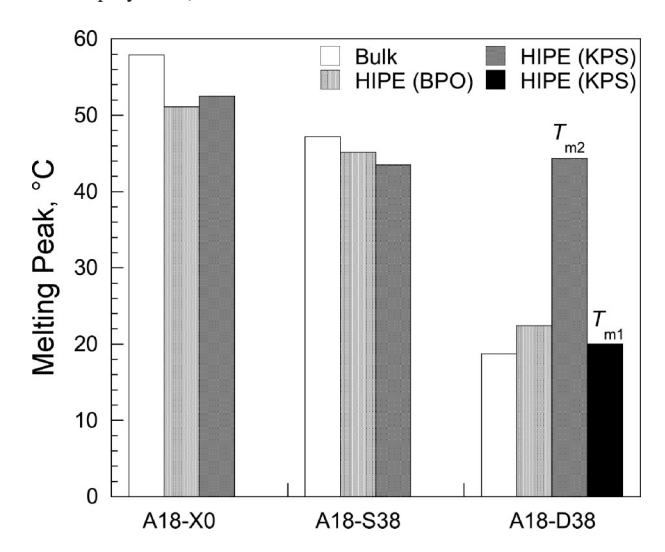


Figure 11. Variation of the melting peak temperatures with the type of synthesis and with the type of comonomer.

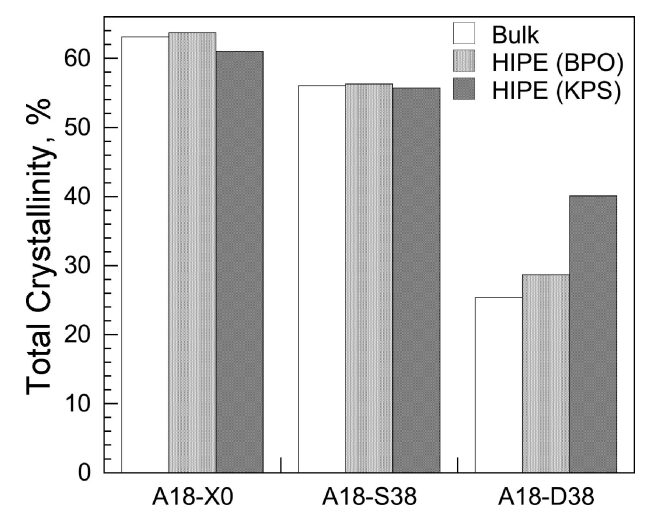


Figure 12. Variation of the total crystallinity with the type of synthesis and with the type of comonomer.

difference between these peak temperatures and  $T_{\rm m2}$  from the interface initiated polymerization is quite significant. Prepolymerized A18-D38-P exhibits a main melting endotherm at 19 °C, similar to those of A18-D38-O and A18-D38-B, and a small additional endotherm at 37 °C, similar to that of A18-D38

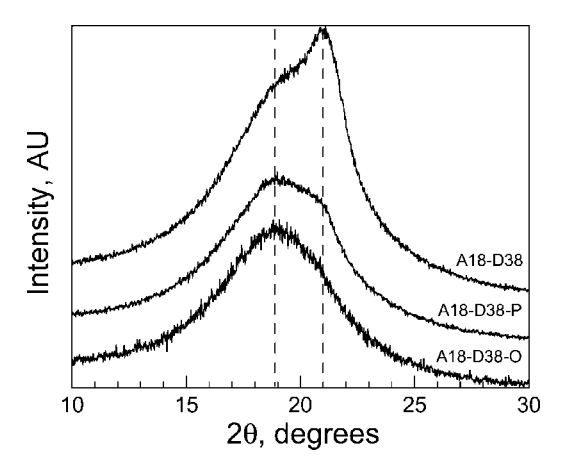


Figure 13. X-ray scattering from various A18-D38-based polyHIPE (standard, prepolymerized, and organic phase initiated).

(Figure 10). While the  $T_{\rm m1}$  peak dominates A18-D38-B, A18-D38-O, and A18-D38-P, it is the  $T_{\rm m2}$  peak that dominates A18-D38. The total crystallinities of organic phase initiated A18-D38-B and A18-D38-O are quite similar and significantly lower than that of interface initiated A18-D38, which has significant contributions to the total crystallinity from both the  $T_{\rm m1}$  and  $T_{\rm m2}$  endotherms (Figure 12).

These results for A18 with 38 mol % DVB indicate that the locus of initiation is integral to the formation of a more highly ordered crystalline structure that has a higher  $T_{\rm m}$ . Initiation at the interface, which is relatively rich in surface active A18, yields enough A18-rich molecular segments to form a more highly ordered crystalline structure. Organic phase initiation, whether in bulk polymerization or in HIPE polymerization, occurs in a random mixture of A18 and DVB. Such a random mixture does not yield enough A18-rich molecular segments to form a more highly ordered crystalline structure. Prepolymerization will yield molecular structures similar to those synthesized using bulk polymerization. However, the interface initiated polymerization that follows prepolymerization will also yield A18-rich molecular segments.

The X-ray spectra from A18-D38-P and A18-D38-O in Figure 13 confirm the DSC results. Neither A18-D38-P nor A18-D38-O exhibits the pronounced crystalline peak at around 21° seen for A18-D38. Both A18-D38-P and A18-D38-O exhibit an amorphous peak at around 18.5° and a very small shoulder at around 21°. The shoulder is more pronounced for A18-D38-P (Figure 13), with its more pronounced melting peak at 37 °C (Figure 10). The compressive stress—strain curves of A18-D38, A18-D38-P, and A18-D38-O in Figure 14 are typical of polyHIPE. The modulus decreases with the decreasing size of the  $T_{\rm m2}$ endotherm, from 1.6 MPa for A18-D38, to 0.9 MPa for A18-D38-P, to 0.2 MPa for A18-D38-O.

Synthesis with a Non-Cross-Linking Comonomer. Copolymerization with DVB can affect the crystallinity through two possible effects. One effect is the disorganization in the regularity of the molecular structure that results from inserting a comonomer into the polymer backbone. A second effect is the formation of cross-links that restrict molecular mobility and tie polymer backbones together. The relative significance of these two effects can be investigated by comparing a crosslinking comonomer, DVB, with an equivalent non-cross-linking comonomer, styrene. The influence of the locus of initiation on the copolymers with styrene can be determined by investigating both interface initiated (A18-S38) and organic phase initiated (A18-S38-O) HIPE polymerizations.

No significant differences between A18-S38 and A18-S38-O could be discerned by comparing their <sup>1</sup>H NMR spectra (not shown). The molecular weights of A18-S38 and A18-S38-O

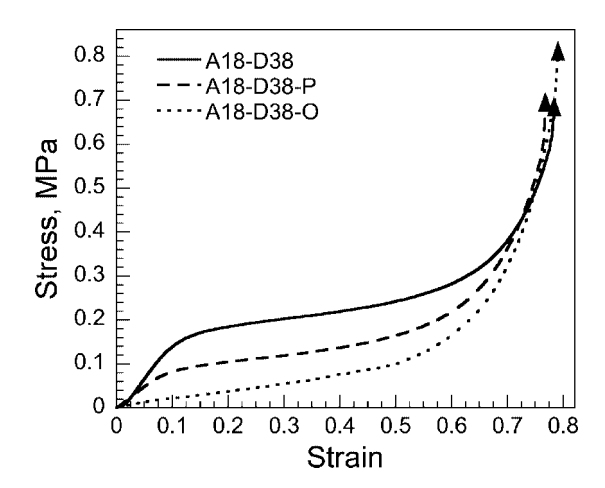


Figure 14. Compressive stress—strain curves for various A18-D38based polyHIPE (standard, prepolymerized, and organic phase initiated).

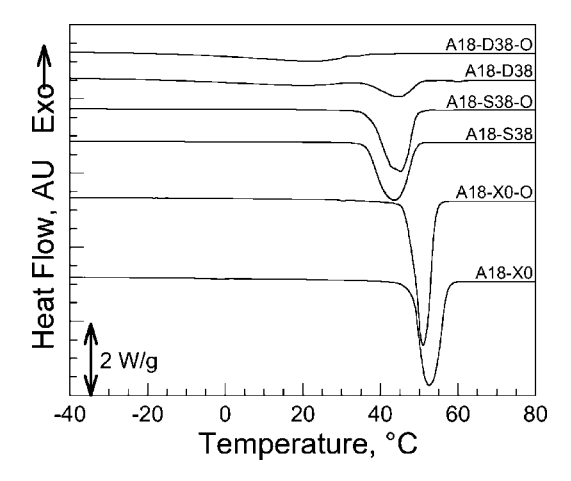


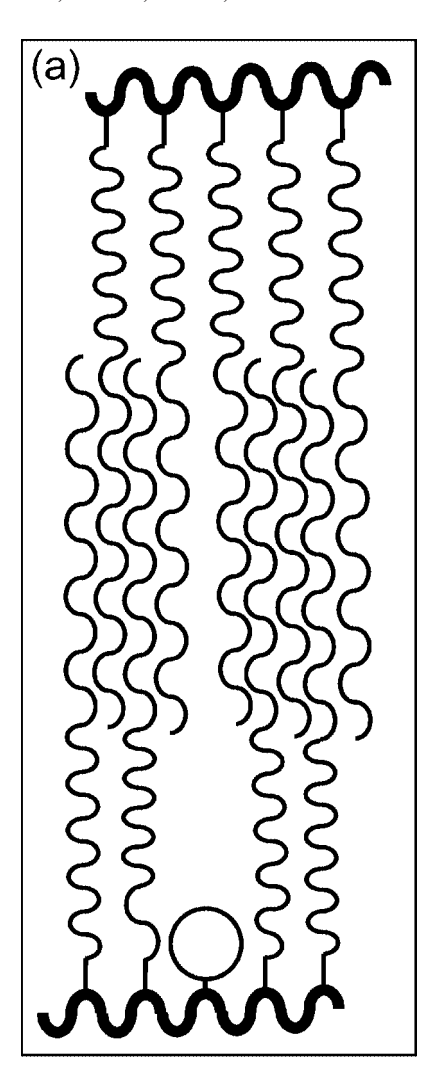
Figure 15. DSC thermograms for A18 homopolymers, copolymers with 38 mol % styrene, and copolymers with 38 mol % DVB for both interface initiated and organic phase initiated polymerizations within HIPE.

Table 3.  $M_n$  and PDI of the Non-Cross-Linked Polymers

	$M_{\rm n}$ , g/mol	PDI
A18-X0	142 000	1.62
A18-X0-O	121 000	2.26
A18-S38	71 000	1.96
A18-S38-O	72 000	2.21

are similar (Table 3), with a slightly lower polydispersity index for interface initiated polymerization. These results indicate that the locus of initiation does not have a significant effect on the molecular structures of the copolymers with styrene. The molecular weights of A18 that was homopolymerized within HIPE, A18-X0 and A18-X0-O, were also determined. The two A18 homopolymer molecular weights were similar (Table 3), with a slightly lower polydispersity index for interface initiated polymerization. The significantly higher molecular weights for the A18 homopolymers may actually reflect the effects that the different molecular structures have on the interactions with the separating column.

The DSC thermograms of A18 homopolymers, copolymers with 38 mol % styrene, and copolymers with 38 mol % DVB for both from interface initiated HIPE polymerizations and from organic phase initiated HIPE polymerizations, are presented in Figure 15. The  $T_{\rm m}$  and  $X_{\rm cT}$  data from Figure 15 are summarized in Figures 11 and 12, respectively. Both the polyHIPE homopolymers exhibit a single melting endotherm with a peak temperature of around 52 °C, somewhat lower than the peak



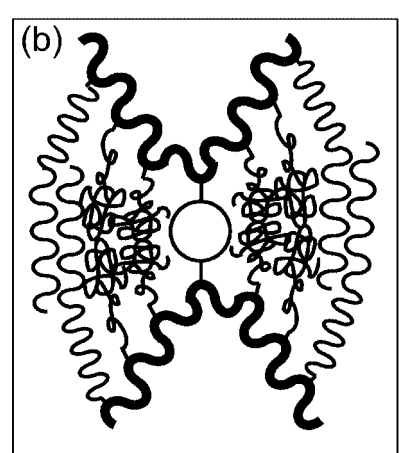


Figure 16. Schematic illustration of interdigitating side chains on incorporation of (a) a non-cross-linking comonomer and (b) a crosslinking comonomer.

temperature of the bulk homopolymer. Copolymerization with styrene does yield a significant reduction in the peak temperature. Both A18-S38 and A18-S38-O exhibit single endotherms with peak temperatures of around 44 °C, quite similar to the  $T_{\rm m2}$  for A18-D38 and to the peak temperature for the bulk copolymer (A18-S38-B). As seen in Figure 11, the locus of initiation in the polyHIPE does not significantly affect the peak temperatures, neither for the homopolymers nor for the copolymers with 38 mol % styrene. The crystallinities for the three homopolymers, around 62%, are not significantly different.

Copolymerization with 38 mol % styrene does produce a significant reduction in crystallinity. The crystallinities of the three copolymers, around 56%, are not significantly different. As seen in Figure 12, the locus of initiation does not seem to significantly affect the crystallinity, neither for the homopolymers nor for the copolymers with 38 mol % styrene.

Unlike the homopolymers and the copolymers with styrene, the locus of initiation does have significant effects on the peak temperatures (Figure 11) and on the total crystallinities (Figure 12) of the copolymers with DVB. Cross-linking produces a significantly greater disruption of the molecular order, yielding significantly lower peak temperatures and significantly lower crystallinities. The differences between a non-cross-linking comonomer and a cross-linking comonomer are emphasized schematically in Figure 16. Cross-linking severely restricts the molecular mobility and the ability of the molecules to rearrange. Cross-linking ties the polymer backbones together and does not allow the backbones to achieve the larger intermolecular distances that are energetically favored for the promotion of side chain crystallization. Copolymerization with styrene does not produce such stringent limitations on molecular mobility, does not tie the polymer backbones together, and, therefore, does not yield such significant reductions in peak temperature and in total crystallinity. Since the significant reductions in peak temperature and in total crystallinity originate in cross-linking, the synthesis of A18-rich molecular segments through initiation at the interface can mitigate the effects of cross-linking and enhance crystallization (Figures 11 and 12). The effects of incorporating a more flexible cross-linking comonomer into A18-based polyHIPE are currently under investigation.

### **Conclusions**

The effects of cross-linking on the crystallinity of stearyl acrylate-based polyHIPE were investigated by varying the comonomer content, by varying the locus of initiation, and by incorporating an equivalent non-cross-linking comonomer.

- The polyHIPE densities were around 0.11 g/cm<sup>3</sup>, as expected from the monomer volume fractions. The porous morphology did not depend strongly on the DVB content.
- Stearyl acrylate-rich molecular segments were formed by polymerization initiated at the organic-water interface, which is relatively rich in the surface active stearyl acrylate. The  $T_{\rm m2}$ endotherm was related to the existence of such stearyl acrylaterich molecular segments. The significant reductions in peak temperatures and in total crystallinity with increasing DVB content were related to cross-linking, which restricts molecular mobility and ties the polymer backbones together. Organic phase initiated polymerization takes place within a random mixture of stearyl acrylate and DVB and, therefore, yields more significant reductions in peak temperatures and crystallinity.
- The decrease in modulus with increasing DVB content for the more crystalline polyHIPE reflects the dominant effect of crystallinity. The increase in modulus with increasing DVB content for the less crystalline polyHIPE reflects the increases in cross-linking and polymer backbone stiffness.

Acknowledgment. The partial support of the Israel Science Foundation and of the Technion VPR Fund is gratefully acknowledged.

## References and Notes

- (1) Barby, D.; Haq, Z. US Pat 4,522,953, 1985.
- (2) Williams, J. M.; Wrobleski, D. A. Langmuir 1988, 4, 656.
- (3) Hainey, P.; Huxham, I. M.; Rowatt, B.; Sherrington, D. C.; Tetley, L. Macromolecules 1991, 24, 117.
- (4) Cameron, N. R.; Sherrington, D. C. J. Mater. Chem. 1997, 7, 2209.
- (5) Cameron, N. R. Polymer 2005, 46, 1439.

- (6) Sergienko, A. Y.; Tai, H.; Narkis, M.; Silverstein, M. S. J. Appl. Polym. Sci. 2004, 94, 2233.
- (7) Leber, N.; Fay, J. D. B.; Cameron, N. R.; Krajnc, P. J. Polym. Sci., Part A: Polym. Chem. 2007, 45, 4043.
- (8) Sergienko, A. Y.; Tai, H.; Narkis, M.; Silverstein, M. S. J. Appl. Polym. Sci. 2002, 84, 2018.
- Tai, H.; Sergienko, A.; Silverstein, M. S. Polym. Eng. Sci. 2001, 41, 1540.
- (10) Kulygin, O.; Silverstein, M. S. Soft Matter 2007, 2, 1525.
- (11) Butler, R.; Davies, C. M.; Cooper, A. I. Adv. Mater. 2001, 13, 1459.
- (12) Butler, R.; Hopkinson, I.; Cooper, A. I. J. Am. Chem. Soc. 2003, 125, 14473.
- (13) Busby, W.; Cameron, N. R.; Jahoda, C. A. B. Biomacromolecules 2001, 2, 154.
- (14) Hayman, M. W.; Smith, K. H.; Cameron, N. R.; Przyborski, S. A. Biochem. Biophys. Methods 2005, 62, 231.
- (15) Hayman, M. W.; Smith, K. H.; Cameron, N. R.; Przyborski, S. A. Biochem. Biophys. Res. Commun. 2004, 314, 483.
- (16) Bokhari, M. A.; Akay, G.; Zhang, S. G.; Birch, M. A. Biomaterials 2005, 26, 5198.
- (17) Akay, G.; Birch, M. A.; Bokhari, M. A. Biomaterials 2004, 25, 3991.
- (18) Busby, W.; Cameron, N. R.; Jahoda, C. A. B. Polym. Int. 2002, 51, 871.
- (19) Lumelski, J.; Zoldan, J.; Levenberg, S.; Silverstein, M. S. Macromolecules 2008, 41, 1469.
- (20) Tai, H.; Sergienko, A.; Silverstein, M. S. Polymer 2001, 42, 4473.
- (21) Silverstein, M. S.; Tai, H.; Sergienko, A. Y.; Lumelsky, Y.; Pavlovsky, S. *Polymer* **2005**, *46*, 6682.
- (22) Normatov, J.; Silverstein, M. S. Polymer 2007, 48, 6648.
- (23) Normatov, J.; Silverstein, M. S. J. Polym. Sci., Part A: Polym. Chem. 2008, 46, 2357.
- (24) Normatov, J.; Silverstein, M. S. Macromolecules 2007, 40, 8329.
- (25) Normatov, J.; Silverstein, M. S. Chem. Mater. 2008, 20, 1571.
- (26) Menner, A.; Powell, R.; Bismarck, A. Soft Matter 2006, 4, 337.

- (27) Haibach, K.; Menner, A.; Powell, R.; Bismarck, A. Polymer 2006, 47, 4513.
- (28) Menner, A.; Haibach, K.; Powell, R.; Bismarck, A. Polymer 2006, 47, 7628.
- (29) Zhang, H.; Hardy, G. C.; Khimyak, Y. Z.; Rosseinsky, M. J.; Cooper, A. I. Chem. Mater. 2004, 16, 4245.
- (30) Livshin, S.; Silverstein, M. S. Macromolecules 2007, 40, 6349.
- (31) Plate, N. A.; Shibaeve, V. P. J. Polym. Sci., Macromol. Rev. 1974, 8, 117.
- (32) Jordan, E. F. J. Polym. Sci., Part A-1: Polym. Chem. 1972, 10, 3347.
- (33) Jordan, E. F.; Feldeise, D. W.; Wrigley, A. N. J. Polym. Sci., Part A-1: Polym. Chem. 1971, 9, 1835.
- (34) Jordan, É. F.; Arthymys, R.; Speca, A.; Wrigley, A. N. J. Polym. Sci., Part A-1: Polym. Chem. 1971, 9, 3349.
- (35) O'Leary, K. A.; Paul, D. R. Polymer 2006, 47, 1226.
- (36) O'Leary, K. A.; Paul, D. R. Polymer 2006, 47, 1245.
- (37) Inomata, K.; Sakamaki, Y.; Nose, T.; Sasaki, S. *Polym. J.* **1996**, 28, 986
- (38) Carnachan, R. J.; Bokhari, M.; Przyborski, S. A.; Cameron, N. R. Soft Matter 2006, 2, 608.
- (39) Yokota, K. In Polymeric Materials Encyclopedia; Salamone, J. C., Ed.; CRC Press: New York, 1996; Vol. 2, p 1342.
- (40) Broadhurst, M. G. J. Res. Natl. Bur. Stand. 1962, 66A, 241.
- (41) Cai, N.; Xu, Y.; Jia, G.; Yuan, C. Polym. Bull. 2007, 59, 491.
- (42) Ouzineb, K.; Graillat, C.; McKenna, T. F. J. Appl. Polym. Sci. 2004, 91, 115.
- (43) Letts, S. A.; Fort, T. J. Colloid Interface Sci. 1998, 202, 341.
- (44) Mumby, S. J.; Swalen, J. D.; Rabolt, J. F. Macromolecules 1986, 19, 1054
- (45) Sato, N.; Sugiura, K.; Ito, S.; Yamamoto, M. Langmuir 1997, 13, 5685.
- (46) Gibson, L. J.; Ashby, M. F. Cellular Solids, 2nd ed.; Cambridge University Press: Cambridge, 1997.

MA800195W